

Interplay between altermagnetism and topological superconductivity in an unconventional superconducting platform

Pritam Chatterjee ^{1, 2, 3, *} and Vladimir Jurićić ^{4, †}

¹*Department of Physics, The University of Tokyo,
7-3-1 Hongo, Bunkyo-ku, Tokyo 113-0033, Japan*

²*Institute of Physics, Sachivalaya Marg, Bhubaneswar-751005, India*

³*Homi Bhabha National Institute, Training School Complex, Anushakti Nagar, Mumbai 400094, India*

⁴*Departamento de Física, Universidad Técnica Federico Santa María, Casilla 110, Valparaíso, Chile*

We propose a theoretical model to investigate the interplay between altermagnetism and p -wave superconductivity, with a particular focus on topological phase transitions in a two-dimensional (2D) p -wave superconductor, considering both chiral and helical phases. Our study reveals that the emergence of helical and chiral Majorana states can be tuned by the amplitude of a d -wave altermagnetic order parameter, with the outcome depending on the nature of the superconducting state. In the helical superconductor, such an altermagnet can induce a topological phase transition into a gapless topological superconductor hosting Majorana flat edge modes (MFEMs). On the other hand, in the chiral superconductor, the topological transition takes place between a topologically nontrivial gapped phase and a gapless nodal-line superconductor, where the Bogoliubov quasiparticle bands intersect at an isolated line in momentum space. Remarkably, we show that when such an altermagnet is coupled to a mixed-pairing superconductor, with both chiral and helical components, a hybrid topological phase emerges, featuring dispersive Majorana edge modes coexisting with nearly flat Majorana edge states. Our findings therefore establish a novel platform for controlling and manipulating Majorana modes in unconventional superconductors with vanishing total magnetization.

I. INTRODUCTION

Altermagnetism, a recently established form of magnetic order, bridges the gap between ferromagnetism and antiferromagnetism [1–3]. While exhibiting zero net magnetization, a characteristic often associated with antiferromagnets, it simultaneously induces spin-split electronic band structures—a hallmark of ferromagnetism. This unique feature has sparked significant interest within both theoretical and experimental condensed matter communities [1–22]. The intriguing nature of altermagnetism extends further since its textures manifest as higher-harmonic orders in momentum space (e.g., d -, f -, g -wave), thus providing the previously lacking magnetic analogs to unconventional superconducting (SC) orders, such as p -, d -, f -wave, etc. This opens exciting avenues for exploring novel material properties and functionalities, which requires further understanding of the underlying mechanisms governing altermagnetism and its potential applications.

The realization of one- and two-dimensional (2D) topological superconductors has been a key impetus in the study of topological phases of matter, driven by the goal of creating localized Majorana zero modes, which are considered as fundamental building blocks for topological quantum computation [23–30]. Furthermore, there has recently been growing interest in gapless topological superconductors from both theoretical and experimental

perspectives [31–39], which may host zero-energy Majorana flat edge modes (MFEMs) instead of isolated Majorana zero modes, with a very recent experiment reporting the signature of MFEMs in a magnetic-superconductor hybrid system composed of Fe/Ta(110) [31]. We here present an alternative approach to introduce gapless topological superconductors hosting MFEMs, along with other new topological superconducting (TSC) phases, by invoking an unconventional SC platform involving an altermagnet, therefore carrying a net zero magnetization, that, to the best of our knowledge, has not been explored until now.

To this end, we here consider the simplest d -wave altermagnetic order parameter (OP) in the presence of both chiral and helical p -wave SC states. We demonstrate that coupling the altermagnetic OP with this unconventional superconductor can give rise to several novel TSC phases. In the case of a helical p -wave superconductor, altermagnetism drives the system from a helical gapped topological superconductor to a gapless topological superconductor that hosts MFEMs. In contrast, for a chiral p -wave superconductor, a topological phase transition occurs, featuring the transition from a chiral gapped p -wave topological superconductor to a gapless nodal-line superconductor in the presence of altermagnetism. Notably, for a mixed p -wave superconductor, combining helical and chiral SC OPs, altermagnetism induces an unusual hybrid topological phase where both dispersive and flat Majorana edge modes coexist. Finally, this work reveals a tunable altermagnet-unconventional-superconductor platform that can support both gapless topological superconductivity, and a hybrid TSC phase that features coexisting dispersive and flat Majorana

* pritam@nt.phys.s.u-tokyo.ac.jp

† vladimir.juricic@usm.cl

edge modes.

The rest of this paper is organized as follows. In Sec. II, we introduce the model for the 2D altermagnet with d -wave magnetic ordering coupled with unconventional helical and chiral p -wave superconductors. Next, we present numerical results on the edge states using the nanoribbon termination in the square lattice geometry in Sec. III, with the results for the edge state spectrum and the local density of states (LDOS) shown in Sec. III A and Sec. III B, respectively, for the chiral and helical phases, while in Sec. III C we discuss both the edge states and LDOS in the case of mixed pairing phase. In Sec. IV, we compute the bulk gap profile as a signature of a topological phase transition by analyzing the corresponding lattice model. Finally, we summarize and discuss our results in Sec. V.

II. MODEL AND METHOD

We here consider the Bogoliubov–de Gennes (BdG) Hamiltonian, representing an interplay between altermagnetism and 2D p -wave superconductor with helical and chiral order that can be written as,

$$H = \frac{1}{2} \sum_{\mathbf{k}} \Phi_{\mathbf{k}}^\dagger h_{\mathbf{k}} \Phi_{\mathbf{k}}, \quad (1)$$

where the four-component Nambu spinor is $\Phi_{\mathbf{k}} = (c_{\mathbf{k}\uparrow}, c_{\mathbf{k}\downarrow}, c_{-\mathbf{k}\uparrow}^\dagger, c_{-\mathbf{k}\downarrow}^\dagger)^\top$, where $c_{\mathbf{k}\uparrow}(c_{\mathbf{k}\downarrow}^\dagger)$ is the annihilation (creation) operator of the quasiparticle at momentum \mathbf{k} and spin up (momentum $-\mathbf{k}$ and spin down), with

$$\begin{aligned} h_{\mathbf{k}} = & \xi_{\mathbf{k}} \tau_z s_0 + J(\mathbf{k}) \tau_0 s_x + \Delta_p^h (\tau_y s_0 \sin k_x - \tau_x s_z \sin k_y) \\ & + \Delta_p^c (\tau_x s_x \sin k_x - \tau_y s_x \sin k_y). \end{aligned} \quad (2)$$

Here, the electron quasiparticle dispersion is $\xi_{\mathbf{k}} = -2t(\cos k_x + \cos k_y) + 4t - \mu$, with μ as the chemical potential. Furthermore, we assume that altermagnetic OP possesses d -wave symmetry,

$$J(\mathbf{k}) = 2J_A (\cos k_x - \cos k_y), \quad (3)$$

with the amplitude of the altermagnetic order J_A [2, 5, 14, 40]. The helical and chiral superconducting OPs are Δ_p^h and Δ_p^c , respectively [41–45]. The Pauli matrices τ_i and s_i , $i = 0, x, y, z$, act on particle-hole space and spin space, respectively. We obtain the spectrum corresponding to the helical superconductor, given by the Hamiltonian in Eq. (2), as

$$\epsilon_{\mathbf{k}} = r \sqrt{\xi_{\mathbf{k}}^2 + J(\mathbf{k})^2 - \frac{1}{2} (\Delta_p^h)^2 (\cos 2k_x + \cos 2k_y)} + s F(\mathbf{k}). \quad (4)$$

For chiral superconductor, on the other hand, since the SC piece of the Hamiltonian commutes with the altermagnetic OP, the spectrum takes the form

$$\epsilon_{\mathbf{k}} = r J(\mathbf{k}) + s \sqrt{\xi_{\mathbf{k}}^2 + (\Delta_p^c)^2 (\sin^2 k_x + \sin^2 k_y)}, \quad (5)$$

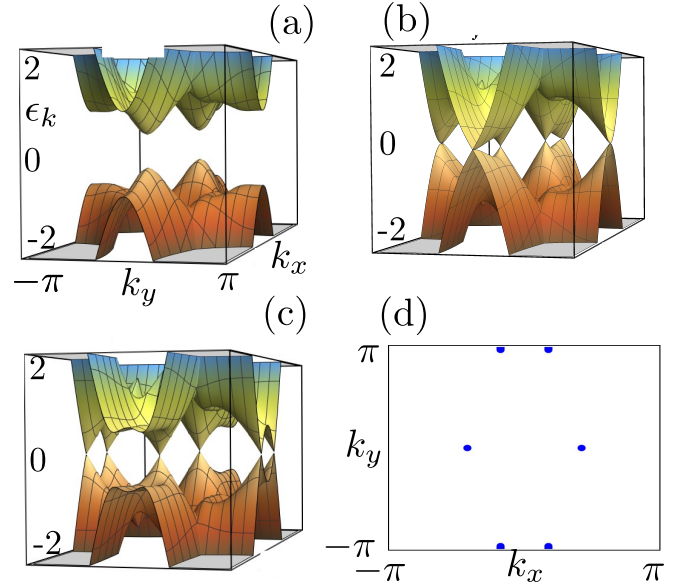


FIG. 1. The band structure for a helical p -wave superconductor coupled to a d -wave altermagnet, as given by Eq. (4). (a) Fully gapped superconducting state for the amplitude of the altermagnetic order parameter $J_A = 0.3t$; (b) Topological phase transition at $J_A = 0.5t$; (c) Nodal superconductor at $J_A = 0.65t$; (d) The nodal Fermi surface plot corresponding to the case (c). The values of parameters are $\mu = 2t$, $\Delta_p^h = t$, and $\Delta_p^c = 0$, with $t = 1$, in Eq. (1).

where $r, s = \pm$ are the band and particle-hole index, respectively. The form of $F(\mathbf{k})$ reads as

$$F(\mathbf{k}) = 2J(\mathbf{k}) \sqrt{\xi_{\mathbf{k}}^2 + (\Delta_p^h \sin k_x)^2}, \quad (6)$$

and the topological phase transitions therefore take place for the critical strength of the altermagnetic OP,

$$J_A^c = \pm \frac{1}{4} |4t - \mu|, \quad (7)$$

with band gap closing at the high-symmetry points $X = (\pi, 0)$ and vice versa.

We show the band structure [Eq. (4)] in Fig. 1 for a helical p -wave superconductor. Notably, a topological phase transition occurs at the amplitude of the altermagnetic OP $J_A = J_A^c$, as given by Eq. (7), separating two distinct topological states. For $J < J_A^c$, the system is always in a gapped, topologically non-trivial phase due to the presence of the helical p -wave superconductivity [see Fig. 1(a)]. In contrast, for $J > J_A^c$, a new topologically non-trivial phase emerges, leading to gapless topological superconductivity [see Fig. 1(c)], which hosts MFEMs. This new phase features an even number of gapless nodes [see Fig. 1(d)], therefore representing a weak topological superconducting phase [46, 47], since it can be viewed as a stack of one-dimensional superconductors in class D (without time-reversal symmetry) changing the topological invariant at the (gapless) nodal points.

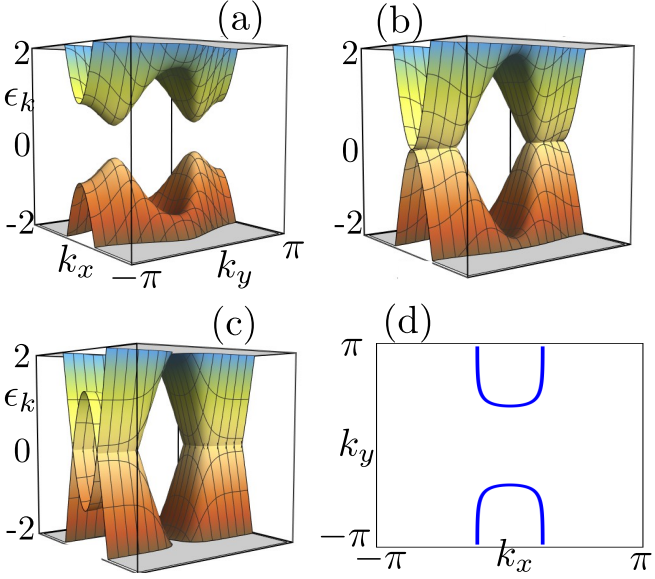


FIG. 2. The band structure for a chiral p -wave superconductor coupled to an altermagnet, as given by Eq. (4). (a) Fully gapped superconducting state for $J_A = 0.3t$; (b) Topological phase transition at $J_A = 0.5t$; (c) Nodal-line superconductor at $J_A = 0.8t$; (d) The nodal Fermi surface plot corresponding to the case (c). The values of parameters are $\mu = 2t$, $\Delta_p^c = t$, and $\Delta_p^h = 0$, with $t = 1$, in Eq. (2).

In Fig. 2, we display the band structure (using Eq. (5)) for a chiral p -wave superconductor. We observe a topological phase transition at $J_A = J_A^c$, where for $J_A < J_A^c$, the system is in a gapped, topologically non-trivial phase with broken time-reversal symmetry. On the other hand, for $J_A > J_A^c$, the system features a gapless nodal line superconductor (see Fig. 2(c)), where the closest to zero energy Bogoliubov quasiparticle bands intersect along a line in the Brillouin zone, with the corresponding form of the Fermi surface displayed in Fig. 2(d). Therefore, for a chiral p -wave superconductor, the d -wave symmetry of the altermagnet drives the system from a gapped topological phase to a gapless nodal line superconductor. In the following section, we discuss the signatures of these nodal superconductors in terms of the edge states.

III. NUMERICAL RESULTS

In this section, we discuss numerical calculations based on the lattice model implemented in real space given by the Hamiltonian in Eq. (1).

A. Edge states in ribbon geometry

The numerical calculations of the edge states in the ribbon geometry are performed by employing periodic boundary conditions (PBC) along the x -direction and open boundary conditions (OBC) along the y -direction.

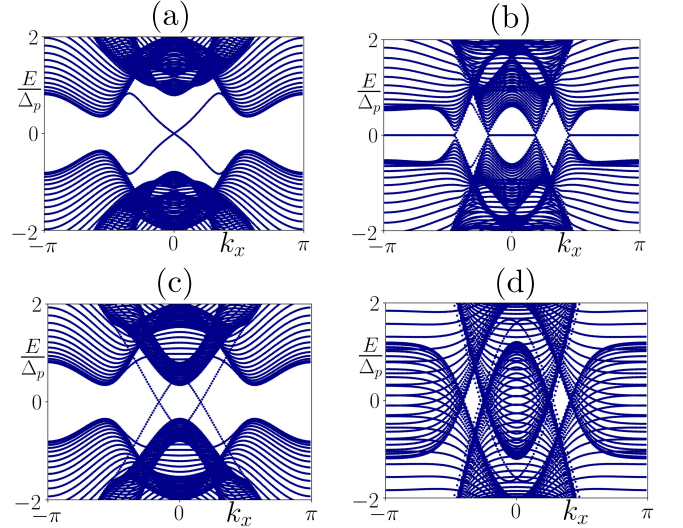


FIG. 3. Edge states in the ribbon geometry for a helical and chiral p -wave superconductor coupled to the altermagnet [Eq. (2)]. (a) [(b)] Helical p -wave superconductor for the altermagnet coupling $J_A = 0.3t$ [$J_A = 0.65t$]. (c) [(d)] Chiral p -wave superconductor for the altermagnet coupling $J_A = 0.3t$ [$J_A = 0.8t$], respectively, for a chiral p -wave superconductor. We employ open [periodic] boundary conditions along y [x] direction and $\mu = 2t$ is fixed.

We first show the spectrum of the edge states for the helical p -wave superconductor for $J_A < J_A^c$ [$J_A > J_A^c$], in Fig. 3(a) [Fig. 3(b)]. For $J_A < J_A^c$, the system exhibits helical edge states protected by time-reversal symmetry, as shown in Fig. 3(a). On the other hand, the system leads to three flat edge modes for $J_A > J_A^c$ [shown in Fig. 3(b)], indicating six gapless points in the momentum space, as displayed in Fig. 1(d). This result closely parallels findings in the study of magnetic textures within hybrid superconductor systems [34], featuring the SC pairing with d -wave symmetry. Notably, in our context, the d -wave symmetry of the altermagnet plays a key role in facilitating gapless topological superconductivity, which is conducive to the emergence of MFEMs in helical p -wave superconductors.

In a chiral p -wave superconductor, the ribbon geometry, as expected, supports two chiral edge channels for a small magnitude of the altermagnet OP $J_A < J_A^c$, as displayed in Fig. 3(c). On the other hand, for the over-critical amplitude, $J_A > J_A^c$, the behavior changes dramatically as the edge modes become delocalized. Such a change in the band structure is a consequence of the transition to a nodal line superconducting phase, characterized by the presence of the isolated lines in the momentum space where the superconducting gap closes. The emergence of this phase is further corroborated by the plot of the corresponding (gapless) nodal lines in Fig. 2(d).

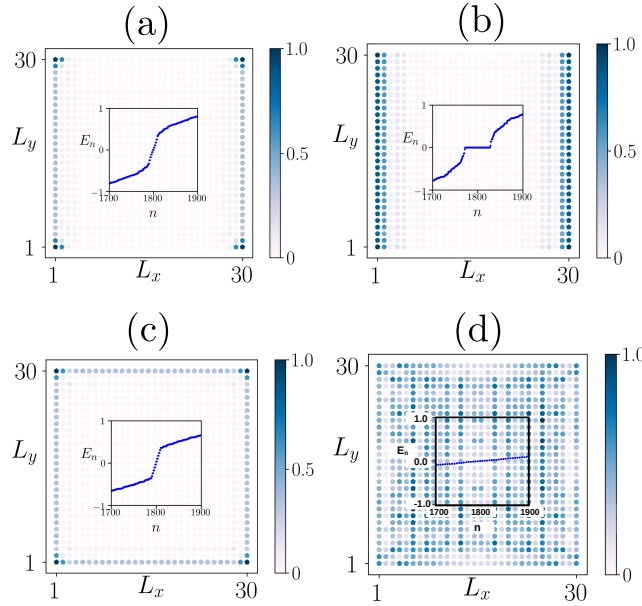


FIG. 4. Panels (a) and (b) show local density of states (LDOS) at zero energy ($E = 0$) of the helical p -wave superconductor coupled to the altermagnet (Eq. (1)) for the values of the altermagnet amplitude $J_A = 0.3t$ and $J_A = 0.65t$, respectively. Panels (c) and (d) display LDOS at $E = 0$ of the chiral p -wave superconductor for the coupling constant $J_A = 0.3t$ and $J_A = 0.8t$, respectively. The inset in each panel shows the spectrum of the closest-to-zero-energy states in the corresponding phase. We here set $\mu = 2t$ and $\Delta_p^h = \Delta_p^c = 1.0$, and $t = 1$.

B. Local density of states

To elucidate the presence of the Majorana modes in this system, we now calculate the LDOS, following the approach outlined in Refs. [32–34]. The quasiparticle LDOS for the i^{th} site at a given energy E reads

$$\rho_i(E) = \sum_{n\sigma} (|u_{i\sigma}^n|^2 + |v_{i\sigma}^n|^2) \delta(E - E_n), \quad (8)$$

where $u_{i\sigma}^n$ and $v_{i\sigma}^n$ are the electronlike and holelike quasiparticle amplitudes, respectively. Here, n and σ are the eigenvalue and spin indices, respectively.

We first consider a helical p -wave superconductor. In Fig. 4, we calculate the LDOS $\rho_i(E)$ at zero energy ($E = 0$) in the xy plane by employing OBC along both the x and y directions, using the lattice Hamiltonian in Eq. (2) in real space. We then find close-to-zero-energy dispersive edge modes that are maximally localized along the two edges of the system for $J_A < J_A^c$, as shown in Fig. 4(a), with the plot of the eigenvalues in the inset of the same figure. In the helical case, altermagnetism drives the system from hosting dispersive Majorana modes in the regime of subcritical altermagnet amplitude to featuring MFEMs when $J_A > J_A^c$. Interestingly, these zero-energy MFEMs are again maximally localized only along the two edges of the system, shown

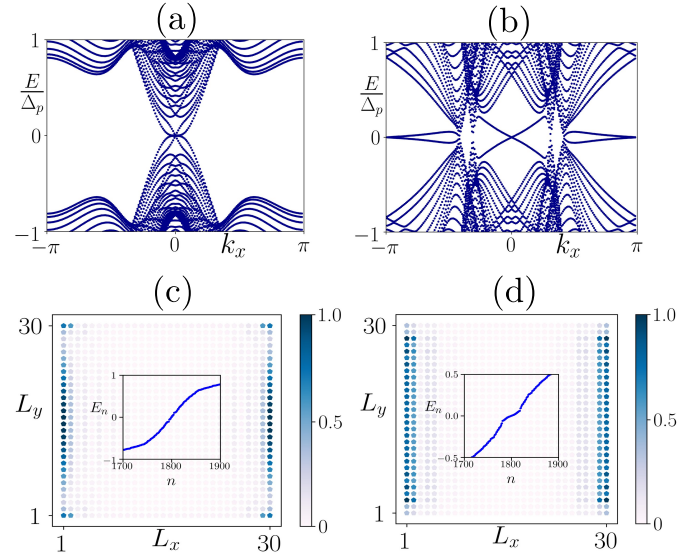


FIG. 5. Nearly flat band edge mode driven by altermagnet in the presence of a mixed helical and chiral superconductor. Panels (a) and (b) show ribbon spectrum for a mixed superconductor when the altermagnet amplitude is below ($J_A < J_A^c$) and above ($J_A > J_A^c$) the critical value (J_A^c) at which the band structure undergoes the transition. Panels (c) and (d) depict corresponding zero energy local density of states for $J_A < J_A^c$ and $J_A > J_A^c$, respectively. We set the parameters $\mu = 2t$ and $\Delta_p^h = \Delta_p^c = t$, with $t = 1$, in Eq. (1).

in Fig. 4(b), with the closest-to-zero-energy modes shown in the inset.

For a chiral p -wave superconductor, when $J_A < J_A^c$, as expected, dispersive Majorana edge modes are highly localized along the four edges of the system, as shown in Fig. 4(c). In contrast, in the case of strong altermagnet OP $J_A > J_A^c$, the edge modes disappear, i.e., they become completely delocalized, as shown in Fig. 4(d), and the bulk enters the nodal line SC phase, consistent with previous analyses of the band structure and the edge states.

C. Mixed topological phase

We now analyze the topological edge states and the LDOS arising from the interplay between d -wave altermagnet and a mixed pairing superconductor with both chiral and helical p -wave components.

In Figs. 5(a) and 5(b), we show the ribbon spectrum calculated under the PBC along the x direction and OBC along the y direction. The spectra reveal dispersive edge modes in the regime of the subcritical altermagnet-superconductor coupling, $J_A < J_A^c$, which are characterized by both linear and quadratic dispersions, as illustrated in Fig. 5(a). Notably, for $J_A > J_A^c$, the system transitions to a mixed topological phase, which supports both linearly dispersing and nearly flat edge modes, as

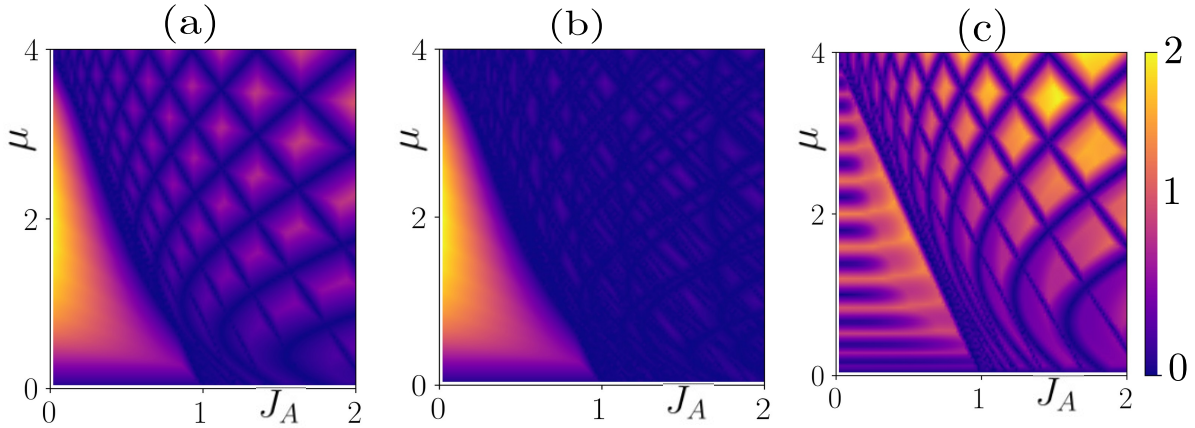


FIG. 6. The bulk gap (Δ) as a function of the chemical potential (μ) and the amplitude of the altermagnet order parameter (J_A) for helical, chiral, and mixed (helical-chiral) p -wave superconductors, shown in panels (a), (b), and (c), respectively. The color bar encodes the size of the gap. We set the parameters $\Delta_p^h = t$ ($\Delta_p^c = t$) in the helical (chiral) phase, while in the mixed phase $\Delta_p^h = \Delta_p^c = t$ in Eq. (1), with $t = 1$. The system size is $N = 30 \times 30$ sites.

depicted in Fig. 5(b). This should be contrasted with the behavior of the edge states observed in the pure chiral and helical superconducting phases, as shown in Fig. 3.

The features of the mixed phase are further corroborated by the $E = 0$ LDOS shown in Figs. 5(c) and 5(d), where the zero-energy state is highly localized along the edges of the finite system, with the closest-to-zero-energy states depicted in the inset. This suggests that the d -wave symmetry of altermagnetism facilitates the formation of this mixed topological phase, which accommodates both dispersive and flat edge states in the presence of mixed helical and chiral p -wave pairings. Such behavior is clearly distinct from that observed in either the purely chiral or helical phase, as can be observed in Fig. 4.

IV. GAP PROFILE

In this section, we analyze the variation of the bulk gap profile by employing PBC along both the x and y directions as a characteristic signature of the topological phase transition.

As an indicator of the topological phase transition, in Fig. 6, we show the maximum value of the gap, $\Delta = |E_2 - E_1|$, between closest to zero energy Bogoliubov quasiparticle bands, where E_1 (E_2) represents the maximum (minimum) of the energy of the negative (positive) energy band. Fig. 6(a) displays the gap, Δ , as a function of the altermagnet strength J_A and chemical potential μ for the helical p -wave superconductor. For a fixed (nonzero) value of μ , we observe that this gapped topologically non-trivial phase remains robust in the regime $J_A < J_A^c$, where J_A^c is the critical coupling for the phase transition at the zero chemical potential. On the other hand, for a strong altermagnet amplitude, $J_A > J_A^c$, we

observe multiple topological phase transitions in terms of the chemical potential, with the bulk gap closing and reopening. Each gap closing point corresponds to a gapless topological superconducting phase hosting MFEMs, as depicted in Fig. 3(b).

In Fig. 6(b), we display the outcome of an analogous analysis for a chiral p -wave superconductor. For a fixed value of μ , we observe a topological phase transition from a topological chiral gapped superconducting phase to a gapless nodal-line superconducting phase, see also Fig. 3(d). Finally, in Fig. 6(c), we show the maximum gap Δ in the $\mu - J_A$ plane for a mixed p -wave superconductor. Interestingly, in this case, we also find multiple topological phase transitions between gapped and gapless phases, which is a clear indication of a mixed topological phase that hosts MFEMs and dispersive edge states, shown in Fig. 5(b).

V. SUMMARY AND DISCUSSION

In summary, we investigated the effect of a d -wave symmetric altermagnet texture on a 2D helical and chiral p -wave superconductor. For a helical p -wave superconductor, altermagnetism drives the system from a helical gapped topological superconductor to a gapless topological superconductor hosting MFEMs. However, for a chiral p -wave superconductor, such a coupling yields a topological phase transition into a gapless nodal line superconductor. Most interestingly, for a mixed (helical-chiral) p -wave superconductor, altermagnetism induces a new hybrid topological phase where dispersive and flat Majorana edge modes coexist.

Our findings, particularly, the predicted gapless topological phase and MFEMs may be relevant in light of a recent experimental proposal [31], where a gapless topolog-

ical superconducting phase hosting MFEMs in a magnet-superconductor heterostructure composed of Fe/Ta(110) has been identified. Here, we propose an alternative method to engineer gapless topological superconductivity hosting MFEMs in an altermagnet and unconventional superconductor hybrid system. Specifically, the potential experimental setup realizing our scenario involves RuO₂, a leading candidate for altermagnetism with *d*-wave magnetic order [1], fabricated on top of a topological *p*-wave superconductor, such as UTe₂ [48]. This heterostructure could serve as a promising candidate for engineering gapless topological superconductivity hosting MFEMs. Although this remains experimentally challenging due to the limited availability of topological *p*-wave supercon-

ducting materials, our study opens new avenues for engineering gapless, and, particularly, hybrid topological SC states, wherein Majorana dispersive and flat edge modes coexist within an unconventional SC platform with zero net magnetization.

Acknowledgments

PC acknowledges Arijit Saha, Kenji Fukushima, and Takashi Oka for fruitful discussions and support. V. J. acknowledges the support of the Swedish Research Council Grant No. VR 2019-04735 and Fondecyt (Chile) Grant No. 1230933.

-
- [1] L. Šmejkal, J. Sinova, and T. Jungwirth, *Phys. Rev. X* **12**, 040501 (2022).
- [2] L. Šmejkal, J. Sinova, and T. Jungwirth, *Phys. Rev. X* **12**, 031042 (2022).
- [3] I. Turek, *Phys. Rev. B* **106**, 094432 (2022).
- [4] P. A. McClarty and J. G. Rau, *Phys. Rev. Lett.* **132**, 176702 (2024).
- [5] S. A. A. Ghorashi, T. L. Hughes, and J. Cano, *Altermagnetic routes to majorana modes in zero net magnetization* (2023), arXiv:2306.09413 [cond-mat.mes-hall].
- [6] M. Papaj, *Phys. Rev. B* **108**, L060508 (2023).
- [7] C. Sun, A. Brataas, and J. Linder, *Phys. Rev. B* **108**, 054511 (2023).
- [8] J. A. Ouassou, A. Brataas, and J. Linder, *Phys. Rev. Lett.* **131**, 076003 (2023).
- [9] D. Zhu, D. Liu, Z.-Y. Zhuang, Z. Wu, and Z. Yan, *Phys. Rev. B* **110**, 165141 (2024).
- [10] S.-B. Zhang, L.-H. Hu, and T. Neupert, *Nature Communications* **15**, 1801 (2024).
- [11] M. Wei, L. Xiang, F. Xu, L. Zhang, G. Tang, and J. Wang, *Phys. Rev. B* **109**, L201404 (2024).
- [12] I. I. Mazin, *Notes on altermagnetism and superconductivity* (2022), arXiv:2203.05000 [cond-mat.supr-con].
- [13] C. W. J. Beenakker and T. Vakhtel, *Phys. Rev. B* **108**, 075425 (2023).
- [14] Y.-X. Li and C.-C. Liu, *Phys. Rev. B* **108**, 205410 (2023).
- [15] C. Sun and J. Linder, *Phys. Rev. B* **108**, L140408 (2023).
- [16] E. W. Hott and J. Linder, *Phys. Rev. B* **109**, 174438 (2024).
- [17] D. Zhu, Z.-Y. Zhuang, Z. Wu, and Z. Yan, *Phys. Rev. B* **108**, 184505 (2023).
- [18] R. M. Fernandes, V. S. de Carvalho, T. Birol, and R. G. Pereira, *Phys. Rev. B* **109**, 024404 (2024).
- [19] S. Das, D. Suri, and A. Soori, *Journal of Physics: Condensed Matter* **35**, 435302 (2023).
- [20] D. Chakraborty and A. M. Black-Schaffer, *Phys. Rev. B* **110**, L060508 (2024).
- [21] D. Mondal, A. Pal, A. Saha, and T. Nag, *Distinguishing between topological majorana and trivial zero modes via transport and shot noise study in an altermagnet heterostructure* (2024), arXiv:2409.08009 [cond-mat.mes-hall].
- [22] S. K. Das and B. Roy, *From local spin nematicity to altermagnets: Footprints of band topology* (2024), arXiv:2403.14620 [cond-mat.mes-hall].
- [23] C.-K. Chiu, J. C. Y. Teo, A. P. Schnyder, and S. Ryu, *Rev. Mod. Phys.* **88**, 035005 (2016).
- [24] M. Sato and Y. Ando, *Reports on Progress in Physics* **80**, 076501 (2017).
- [25] C. Nayak, S. H. Simon, A. Stern, M. Freedman, and S. Das Sarma, *Rev. Mod. Phys.* **80**, 1083 (2008).
- [26] R. M. Lutchyn, J. D. Sau, and S. Das Sarma, *Phys. Rev. Lett.* **105**, 077001 (2010).
- [27] S. Nadj-Perge, I. K. Drozdov, B. A. Bernevig, and A. Yazdani, *Phys. Rev. B* **88**, 020407 (2013).
- [28] X.-L. Qi, T. L. Hughes, and S.-C. Zhang, *Phys. Rev. B* **82**, 184516 (2010).
- [29] A. Saha and A. M. Jayannavar, *Resonance* **22**, 787 (2017).
- [30] P. Chatterjee, S. Pradhan, A. K. Nandy, and A. Saha, *Phys. Rev. B* **107**, 085423 (2023).
- [31] R. Brüning, J. Bedow, R. L. Conte, K. von Bergmann, D. K. Morr, and R. Wiesendanger, *The non-collinear path to topological superconductivity* (2024), arXiv:2405.14673 [cond-mat.supr-con].
- [32] P. Chatterjee, S. Banik, S. Bera, A. K. Ghosh, S. Pradhan, A. Saha, and A. K. Nandy, *Phys. Rev. B* **109**, L121301 (2024).
- [33] P. Chatterjee, A. K. Ghosh, A. K. Nandy, and A. Saha, *Phys. Rev. B* **109**, L041409 (2024).
- [34] M. Subhadarshini, A. Pal, P. Chatterjee, and A. Saha, *Applied Physics Letters* **124**, 183102 (2024).
- [35] S. Nakosai, Y. Tanaka, and N. Nagaosa, *Phys. Rev. B* **88**, 180503 (2013).
- [36] N. Sedlmayr, J. M. Aguiar-Hualde, and C. Bena, *Phys. Rev. B* **91**, 115415 (2015).
- [37] P. Wang, S. Lin, G. Zhang, and Z. Song, *Scientific Reports* **7**, 17179 (2017).
- [38] K. L. Zhang, P. Wang, and Z. Song, *Scientific Reports* **9**, 4978 (2019).
- [39] W. Chen and A. P. Schnyder, *Phys. Rev. B* **92**, 214502 (2015).
- [40] L. Šmejkal, A. H. MacDonald, J. Sinova, S. Nakatsuji, and T. Jungwirth, *Nature Reviews Materials* **7**, 482 (2022).
- [41] M. Amundsen and V. Jurić, *Phys. Rev. Res.* **4**, 013088 (2022).

- [42] Y. Wang, M. Lin, and T. L. Hughes, *Phys. Rev. B* **98**, 165144 (2018).
- [43] Z. Wu, Z. Yan, and W. Huang, *Phys. Rev. B* **99**, 020508 (2019).
- [44] X. Zhu, *Phys. Rev. Lett.* **122**, 236401 (2019).
- [45] A. P. Schnyder and S. Ryu, *Phys. Rev. B* **84**, 060504 (2011).
- [46] L. Fu, C. L. Kane, and E. J. Mele, *Phys. Rev. Lett.* **98**, 106803 (2007).
- [47] J. E. Moore and L. Balents, *Phys. Rev. B* **75**, 121306 (2007).
- [48] L. Jiao, S. Howard, S. Ran, Z. Wang, J. O. Rodriguez, M. Sigrist, Z. Wang, N. P. Butch, and V. Madhavan, *Nature* **579**, 523 (2020).